ACS OMEGA

http://pubs.acs.org/journal/acsodf

Article

Sensing Mechanism of H_2O, NH_3, and O_2 on the Stability-Improved $Cs_2Pb(SCN)_2Br_2$ Surface: A Quantum Dynamics Investigation

Bing Zhang, Xiaogang Wang, Yang Yang, Bin Hu, Lei Tong, Ying Liu, Li Zhao, and Qiang Lu*

Cite This: *ACS Omega* 2021, 6, 24244−24255

Read Online

ACCESS | Metrics & More | Article Recommendations | Supporting Information

ABSTRACT: Although the perovskite sensing materials have shown high sensitivity and ideal selectivity toward neutral, oxidative, or reductive gases, their structural instability hampers the practical application. To exploit perovskite-based gas-sensing materials with improved stability and decent sensitivity, three adsorption complexes of H_2O, NH_3, and O_2 on the $Cs_2Pb(SCN)_2Br_2$ surface are built by doping Br^- and Cs^+ in the parent $(CH_3NH_3)_2Pb(SCN)_2I_2$ structure and submitted to quantum dynamics simulations. Changes in the semiconductor material geometric structures during these dynamic processes are analyzed and adsorption ability and charge transfer between $Cs_2Pb(SCN)_2Br_2$ and the gas molecules are explored so as to further establish a correlation between the geometrical structure variations and the charge transfer. By comparing with the previous $CH_3NH_3PbI_3$ and $(CH_3NH_3)_2Pb(SCN)_2I_2$ adsorption systems, we propose the key factors that enhance the stability of perovskite structures in different atmospheres. The current work is expected to provide clues for developing innovative perovskite sensing materials or for constructing reasonable sensing mechanisms.

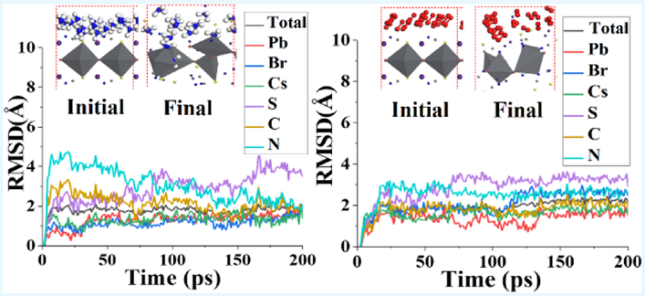

1. INTRODUCTION

The metal−organic halide perovskite ABX_3 has attracted much interest due to its excellent photovoltaic properties.[1−5] At present, the power conversion efficiency (PCE) of solar cells based on ABX_3 structures has exceeded 25.5%;[6] however, the structural instability of perovskite materials hinders their further development and application in solar cells.[7−10] Zhao[11] and Bao[12] et al. used $CH_3NH_3PbI_3$ to explore the gas-sensing properties of NH_3, which usher in an era of applying perovskite materials in gas sensing. Since then, the detection limit of O_2 concentration has been reduced to as low as 70 ppm based on $CH_3NH_3PbI_3$ films,[13] while $CH_3NH_3PbI_{3-x}Cl_x$ has been proved to be able to detect an ultralow ozone concentration of few ppb.[14] These typical experiments have proved the extraordinary sensitivity of the perovskite materials to gases with different reductive or oxidative properties.[11−18] Differing from the application in solar cells, the range for designing stable perovskite materials for gas sensing can break through the strict limitations on band gaps of photovoltaic materials and hence the interest in the development of such perovskite materials has been triggered.

Despite the extraordinary sensitivity or selectivity of $CH_3NH_3PbI_3$ to gases with various physical or chemical properties, it has been found that the sensing material could be damaged when putting in NH_3 (reductive), H_2O (neutral), and O_2, NO_2, or O_3 (oxidative) environment. The stability improvement of the gas sensors based on perovskite materials, therefore, remains a major challenge. Our previous quantum dynamics simulations show that Pb^{2+} with an intermediate valence state exhibits both reduction and oxidation ability, thus it offers active sites that are attacked by both oxidizing and reducing gases, and the weak Pb−I framework fails to resist attack by strong oxidative or reductive gases. Further experiments have proved that $(CH_3NH_3)_2Pb(SCN)_2I_2$, obtained through the partial substitution of the X-site elements in $CH_3NH_3PbI_3$, can improve the perovskite material moisture resistance.[19] In the simulations of $(CH_3NH_3)_2Pb(SCN)_2I_2$ adsorbing gases with different properties, i.e., neutral H_2O, reductive NH_3, and oxidative NO_2, O_2, and O_3, it is found what underpins the mechanism of the SCN^- groups effectively enhancing the stability of perovskite skeletons is that both the S atoms and the CN groups of SCN^- can stably bond with Pb. Therefore, the structural stability in the dynamics process is maintained in the form of Pb−NCS or Pb−SCN−Pb network structures. However, the weak Pb−I bonds in the structure are still the targets of oxidizing or reducing gases. It has been found that both the neutral H_2O and oxidative gases (NO_2, O_2, and O_3) can form a stable Pb−O connection by directly attacking the Pb−I bonds.[20] Anyway, in the study of the adsorption of reductive NH_3 by $CH_3NH_3PbI_3$,[21] it is found

Received: August 3, 2021
Accepted: August 24, 2021
Published: September 3, 2021

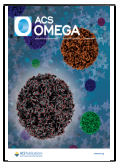

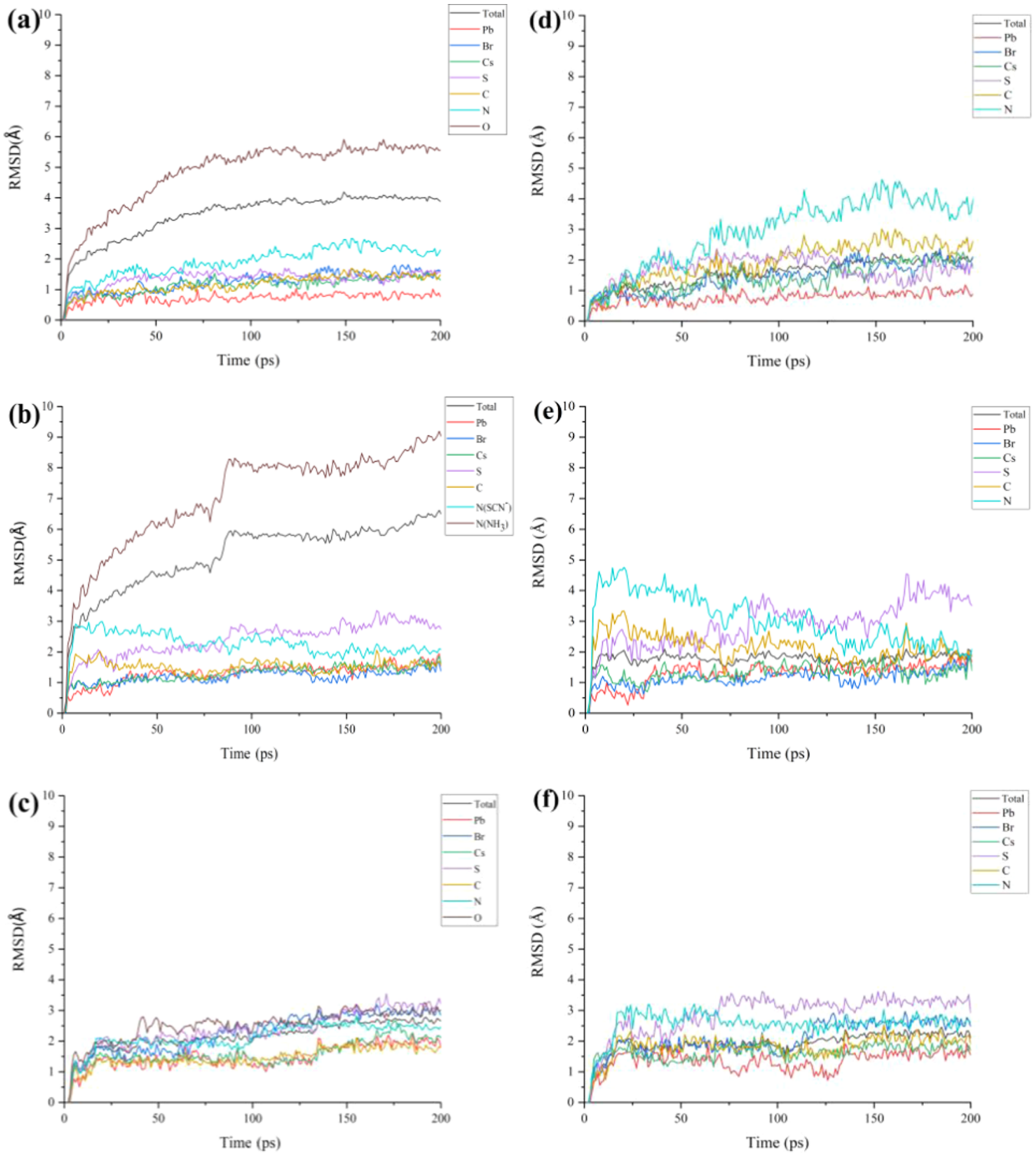

Figure 1. Curves in (a)−(c) are the RMSD of the $Cs_2Pb(SCN)_2Br_2$−H_2O (a), $Cs_2Pb(SCN)_2Br_2$−NH_3 (b), and $Cs_2Pb(SCN)_2Br_2$−O_2 (c) complexes, respectively. (d)−(f) Fluctuations of atoms on the $Cs_2Pb(SCN)_2Br_2$ surface in complexes (a)−(c), respectively.

that the A-site $CH_3NH_3^+$ groups rapidly adsorb NH_3 and undergo H proton exchanges, thus blocking the interactions between the gas molecules and the skeletons; nevertheless, NH_3 can eventually break through the $CH_3NH_3^+$ barrier and interact with Pb to achieve stable adsorption and charge exchange. In addition, during the adsorption process, it has been confirmed that the perovskite materials normally receive charges from reductive gases but donate charges to oxidative gases, which is believed to be related to the electron structural changes of the semiconducting materials.[21]

In recent years, the substitution of the original A-site organic groups with inorganic elements or groups to improve the perovskite stability has also been utilized in gas sensing. Experiments have proved that $Cs_2Pb(SCN)_2I_2$ exhibits enhanced ambient stability compared with $(CH_3NH_3)_2Pb(SCN)_2I_2$.[22] In addition, $CsPbBr_3$ has been used to detect

https://doi.org/10.1021/acsomega.1c03952
ACS Omega 2021, 6, 24244−24255

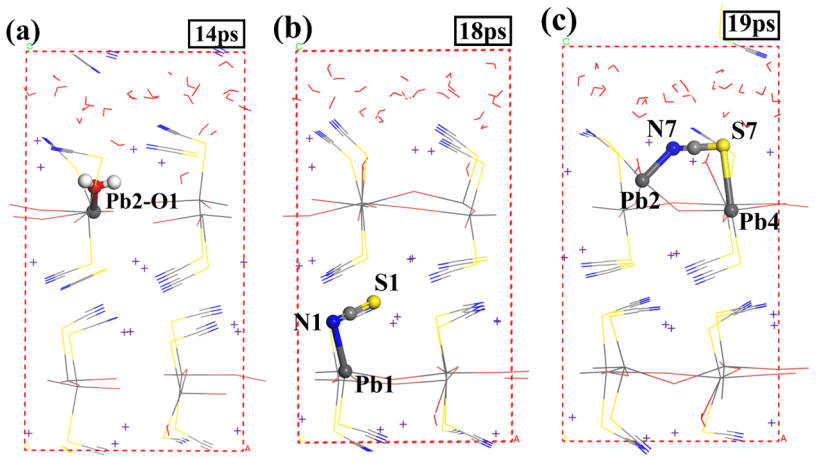

Figure 2. Typical snapshots during the $Cs_2Pb(SCN)_2Br_2-H_2O$ simulations: (a) Pb and OH_2 connection, (b) formation of a Pb−NCS bond, and (c) formation of a Pb−SCN−Pb network.

volatile organic compounds (acetone and ethanol) with a detection limit as low as 1 ppm. In addition, it also provides a fast response and rapid recovery in the detection of O_2.[23] The excellent stability of $CsPbBr_3$ in air and oxygen has also been verified.[24]

Investigating the gas-sensing mechanisms is the first step leading to the development of ideal sensing materials, while research on adsorption and desorption of gas molecules on the perovskite material surface is the starting point for probing gas-sensing mechanisms. According to Yamazoe[25] et al., the initial move in the sensing process of semiconductor−gas molecules is to calibrate gas molecules and their active sites where the gas operates via the electronic changes introduced by gas−solid interactions. Our previous work[20,21] shows that the structural instability of the perovskite materials causes different dynamic changes around the adsorption sites. Such a property challenges the traditional static first-principles calculations;[26−33] therefore, the quantum dynamics methodology is employed to deal with such special properties.[20,21,34−39]

In the current work, to improve the structural stability of $CH_3NH_3PbI_3$ and to clarify the sensing mechanism origin of the perovskites toward gases with different oxidation−reduction characteristics, the original organic $CH_3NH_3^+$ groups are replaced by inorganic Cs^+ and the weak Pb−I bonds are substituted by Pb−SCN and Pb−Br. The previously simulated typical neutral (H_2O), reductive (NH_3), and oxidative (O_2) gases are reselected to form three complexes of $Cs_2Pb(SCN)_2Br_2-H_2O$, $Cs_2Pb(SCN)_2Br_2-NH_3$, and $Cs_2Pb(SCN)_2Br_2-O_2$, respectively. All of the systems are submitted to dynamics simulations. The structural stability of $Cs_2Pb(SCN)_2Br_2$, under the attack of strong reductive, oxidative, and neutral gas molecules, is described in detail via monitoring the bond breaking and formation during the dynamics processes. The adsorption energy and charge transfer between the perovskite materials and the gases are both quantified. The adsorption details of H_2O, NH_3, and O_2 with $CH_3NH_3PbI_3$ and $(CH_3NH_3)_2Pb(SCN)_2I_2$ are also recalled and compared with systems in the current work. Based on the comparisons, a relationship between the geometrical structure changes of the semiconductor materials and the charge transfer is established. The purpose of this research is to reveal the adsorption−desorption processes and the stability enhancement mechanisms of $Cs_2Pb(SCN)_2Br_2$ in an environment containing gases bearing different properties, so as to provide new ideas for developing perovskite sensing materials with improved stability and decent sensitivity.

2. RESULTS AND DISCUSSION

The root mean square deviations (RMSDs) of all of the complexes are demonstrated in Figure 1. The RMSD curves of the $Cs_2Pb(SCN)_2Br_2-H_2O$, $Cs_2Pb(SCN)_2Br_2-NH_3$, and $Cs_2Pb(SCN)_2Br_2-O_2$ systems tend to be stable at 125, 95, and 145 ps, respectively, indicating that the adsorption of the gas molecules on the perovskite skeletons reaches an equilibrium. It takes different time spans for the RMSD curves of the three systems to obtain an equilibrium, and the fluctuations of which are distinct as well, which might suggest that gases with different chemical properties exhibit different adsorption behaviors. The RMSD of the atoms on the perovskite material surface, including Pb, Br, S, C, and N, have also been extracted and described in Figure 1. From the figure, it is clear that the fluctuations of S, C, and N on the surface are larger than those of the atoms inside the skeleton. This is in agreement with the structural stability analyses below, where the −SCN groups on the surface stick out to and are disturbed by the gas molecules to form new Pb−SCN−Pb connections.

2.1. Adsorption Properties of Water Molecules on the $Cs_2Pb(SCN)_2Br_2$ Surface. The simulations show that, compared with those of the $CH_3NH_3PbI_3$ and $(CH_3NH_3)_2Pb(SCN)_2I_2$ systems, the stability of $Cs_2Pb(SCN)_2Br_2$ is further improved in a humid environment. The study of the adsorption of H_2O on $CH_3NH_3PbI_3$ and $(CH_3NH_3)_2Pb(SCN)_2I_2$ demonstrates that the breakage of the weak Pb−I bonds in the dynamic process is the main reason for the distortion and collapse of the perovskite skeletons under the attack of water molecules. Therefore, in the current work, the changes in the Pb−Br bonds in $Cs_2Pb(SCN)_2Br_2$ are first investigated. In the current dynamics process, a Pb−I connection is considered broken when the bond length is stretched longer than 3.4 Å and the threshold is 3.25 Å for a Pb−Br connection.[40] At the end of the simulations, there are 21 intact Pb−Br bonds, out of the initial 32 bonds in the system, and the integrity rate is 65.63% (21/32). The integrity rates of Pb−I bonds in the $(CH_3NH_3)_2Pb(SCN)_2I_2$ and $CH_3NH_3PbI_3$ systems are 62.50% (20/32) and 58.33% (28/48), respectively. Therefore, the substitution of the original

https://doi.org/10.1021/acsomega.1c03952
ACS Omega 2021, 6, 24244−24255

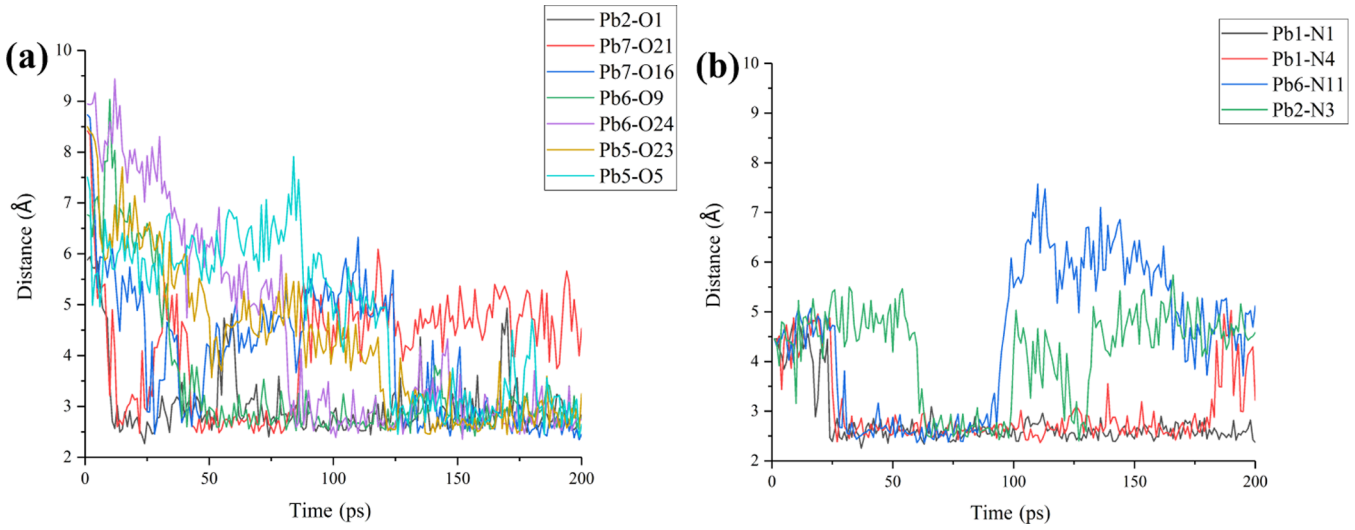

Figure 3. Changes in the new connections in the $Cs_2Pb(SCN)_2Br_2-H_2O$ system: (a) Pb−O interaction and (b) Pb−NCS connection.

Pb−I bonds with stronger Pb−Br connections can effectively decrease the broken Pb−X bond proportion, thus reducing the opportunity for the exposed metal ions to connect with H_2O molecules. Anyway, a small portion of the Pb−Br bonds are still broken under the attack of H_2O molecules, and H_2O is found to attack Pb atoms and form Pb2−O1, Pb7−O21, Pb7−O16, Pb6−O9, Pb6−O24, Pb5−O23, and Pb5−O5 connections (Figure 2a). The distances between these Pb and O atoms are mostly slightly longer than the Pb−O bond length (2.49 Å),[41] indicating that the interactions between Pb−OH_2 are weaker than that of normal Pb−O bonds (Figure 3a). In the simulations of $CH_3NH_3PbI_3-H_2O$ and $(CH_3NH_3)_2Pb(SCN)_2I_2-H_2O$, the release of reactants CH_3NH_3I and CH_3NH_3SCN is observed at 5 and 94 ps (Figure 4),

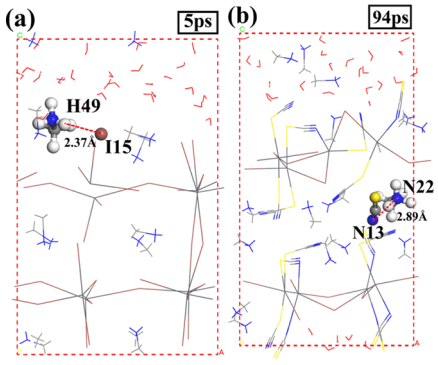

Figure 4. Release of the reactants (a) CH_3NH_3I and (b) CH_3NH_3SCN.

respectively; no reactant is, however, observed in the $Cs_2Pb(SCN)_2Br_2-H_2O$ system. This implies that the doping of SCN^- and Br^- is conducive to improving the perovskite structural stability.

Furthermore, it has been proved that the formation of stable Pb−NCS bonds and Pb−SCN−Pb networks in the $(CH_3NH_3)_2Pb(SCN)_2I_2$ system is the crucial reason to effectively maintain the stability of perovskite structures. In the $Cs_2Pb(SCN)_2Br_2-H_2O$ complex, it is also noticed that SCN^- groups rotate in the dynamic process to form Pb−NCS bonds (Figure 2b). In view of this phenomenon, the structures of $Cs_2Pb(SCN)_2Br_2$ and $Cs_2Pb(NCS)_2Br_2$ are both optimized, and the formation energies are −124.475 eV and −124.050 eV, respectively (Figure 5). These energies are very similar,

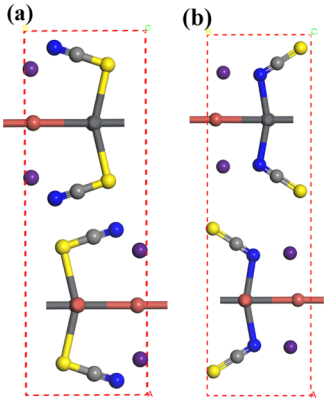

Figure 5. Structural optimization of (a) Pb−SCN and (b) Pb−NCS connections.

revealing that both connections can exist stably. Furthermore, Pb1−(NCS)4, Pb6−(NCS)11, and Pb2−(NCS)3 connections are successively observed (Figure 3b). Moreover, the Pb4−(SCN)7−Pb2 network is also detected at 19 ps (Figure 2c).

The stability improvement mechanisms of the perovskite structure by replacing the polar stick-like $CH_3NH_3^+$ groups with the nonpolar spherical CS^+ atoms have been proved previously. The rotation of the former is shown to damage the weak Pb−I bonds in three-dimensional (3D) skeletons to a certain extent.[40] Li et al.[22] suggested that when CS^+ is inserted into a two-dimensional (2D) $(PbX_4(SCN)_2)$ framework, smaller Br^- that is more strongly bonded with Pb^{2+} can be used, without serious lattice distortion in air, which is also verified by our simulation results. The comparison of the dynamic fluctuations of the three systems shows that the amplitude of fluctuation of Cs^+ in the $Cs_2Pb(SCN)_2Br_2-H_2O$ system is much smaller than that of $CH_3NH_3^+$ in the $CH_3NH_3PbI_3-H_2O$ and $(CH_3NH_3)_2Pb(SCN)_2I_2-H_2O$ complexes (Figure S1). In addition, the increased amplitudes of the RMSD curves of Pb and Br atoms are smaller than those of Pb and I in the $CH_3NH_3PbI_3-H_2O$ and $(CH_3NH_3)_2Pb$-

https://doi.org/10.1021/acsomega.1c03952
ACS Omega 2021, 6, 24244−24255

$(SCN)_2I_2$−H_2O systems, indicating that the substitution of Cs^+ can stabilize such materials.

2.2. Adsorption Properties of NH_3 on the $Cs_2Pb(SCN)_2Br_2$ Surface. The dynamics results show that without the blockage of $CH_3NH_3^+$, NH_3 can rapidly and directly attack Pb atoms on the $Cs_2Pb(SCN)_2Br_2$ surface, which is the biggest difference between the $Cs_2Pb(SCN)_2Br_2$−NH_3 system and the previous $CH_3NH_3PbI_3$−NH_3 system. On the $CH_3NH_3PbI_3$ surface, NH_3 molecules do not stably bond with Pb atoms until 150 ps.[21] Meanwhile, the CH_3NH_2 groups, the products of $CH_3NH_3^+$−NH_3 proton exchange, attack Pb atoms to form a Pb−N connection, which survives the rest of the simulations. These Pb−NH_2CH_3 bonds rotate continuously to break the nearby Pb−I bonds, which directly leads to the damage of the Pb−I skeleton. The reactant CH_3NH_3I has been observed at 5 ps, as seen in Figure 6. In the current system, the bond length

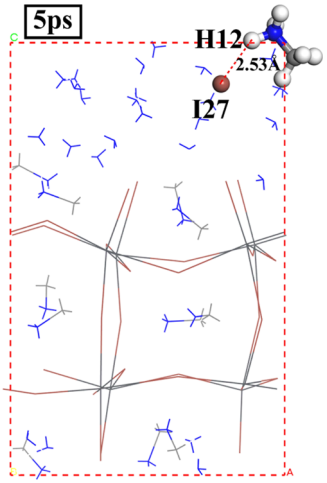

Figure 6. Release of the reactant CH_3NH_3I in the $CH_3NH_3PbI_3$−NH_3 complex.

of Pb5-N17 reaches 2.41 Å at 20 ps (Figure 7a), which is smaller than the standard Pb−N bond length of 2.91 Å.[42] After that, stable connections of Pb3−N36, Pb6−N23, Pb8−N35, and Pb6−N30 are successively generated at 21, 29, 51, and 60 ps, respectively (Figure 8). Pb6−N30 is formed at 60 ps and remains stable until the end of the simulation, and no new Pb−

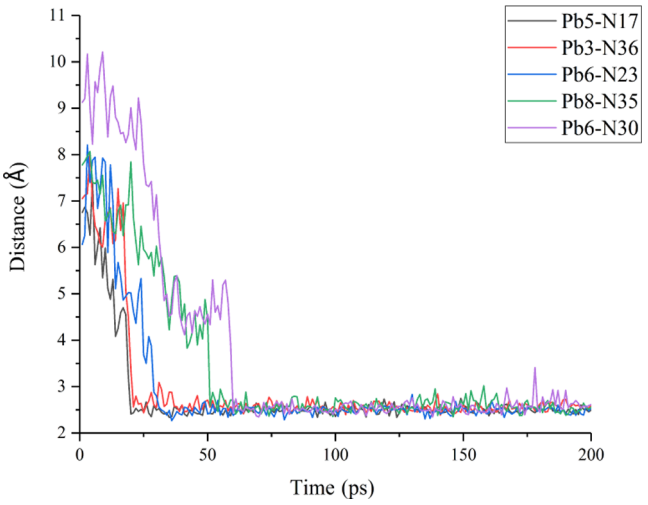

Figure 8. Connection of Pb and NH_3 in the $Cs_2Pb(SCN)_2Br_2$−NH_3 complex.

N connections are observed. The Pb−NH_3 bonding does not rotate like Pb−NH_2CH_3 in the $CH_3NH_3PbI_3$−NH_3 complex, while the Pb−Br bonds are only partially broken. Therefore, the octahedrons in the perovskite skeletons remain intact without serious distortion or collapse (Figure 9b). At the end of the simulations, the integrity rate of the Pb−Br bonds in the $Cs_2Pb(SCN)_2Br_2$−NH_3 system is 71.88% (23/32), while that in the $CH_3NH_3PbI_3$−NH_3 complex is 56.25% (27/48).

In addition, both the Pb−NCS and Pb−SCN−Pb networks have been observed in the $Cs_2Pb(SCN)_2Br_2$−NH_3 system (Figure 7b), which also make contributions to improving the stability of the perovskite structures.

2.3. Adsorption Properties of O_2 on the $Cs_2Pb(SCN)_2Br_2$ Surface. In contrast to H_2O and NH_3 that can form stable interactions with exposed lead atoms, the O_2 molecules on the perovskite surface are found to be frequently adsorbed and desorbed. As shown in Figure 10a, the distance

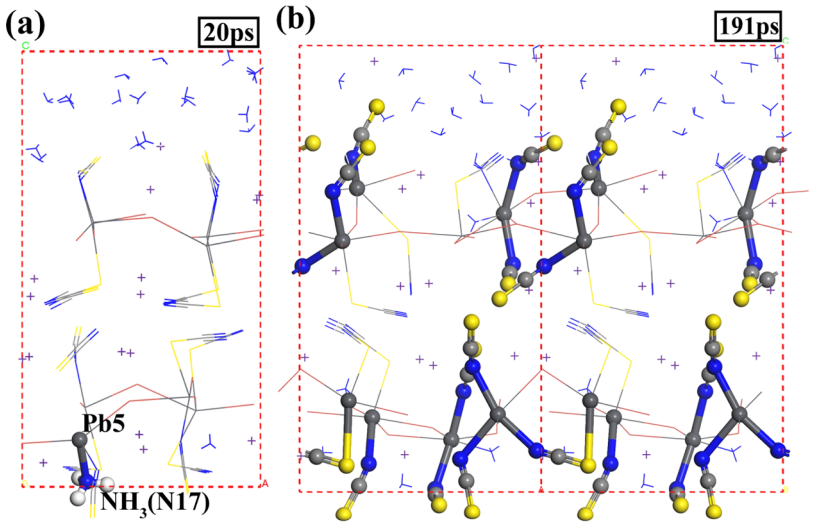

Figure 7. Typical snapshots of the $Cs_2Pb(SCN)_2Br_2$−NH_3 complex in the current work: (a) Pb and NH_3 connection and (b) formation of Pb−NCS and Pb−SCN−Pb networks.

https://doi.org/10.1021/acsomega.1c03952
ACS Omega 2021, 6, 24244−24255

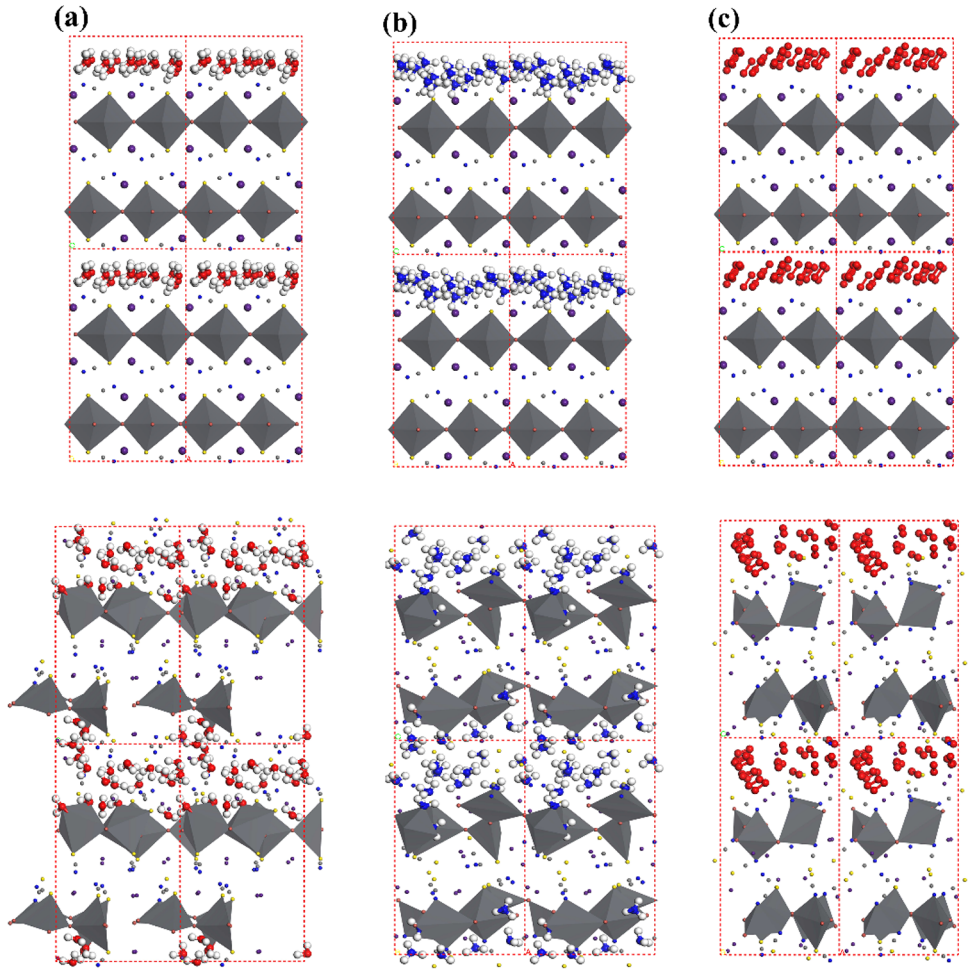

Figure 9. Starting and final structures of the adsorption systems: (a) $Cs_2Pb(SCN)_2Br_2-H_2O$, (b) $Cs_2Pb(SCN)_2Br_2-NH_3$, and (c) $Cs_2Pb(SCN)_2Br_2-O_2$.

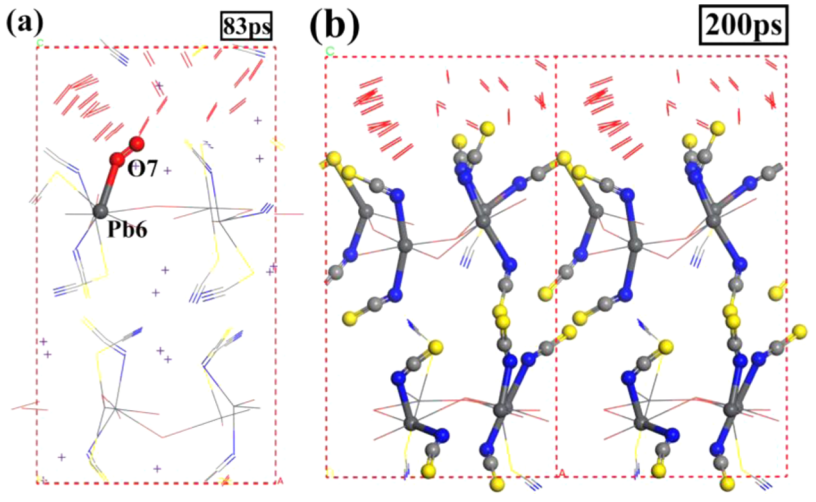

Figure 10. Typical snapshots of the $Cs_2Pb(SCN)_2Br_2-O_2$ complex: (a) weak Pb−O_2 connection and (b) Pb−NCS and Pb−SCN−Pb networks.

of the Pb6-O7 connection is 2.59 Å at 83 ps, which is longer than the Pb−O bond length of 2.49 Å,[41] suggesting a weak interaction between Pb6 and O7 (Figure 11a). Such adsorption properties of O_2 are also observed on the surfaces of $CH_3NH_3PbI_3$ and $(CH_3NH_3)_2Pb(SCN)_2I_2$; however, in these two systems, the O_2 molecules manage to enter the perovskite lattices by attacking and breaking the Pb−I bonds to temporarily bond with Pb^{2+}, which severely damages the material structures (Figure S2). In this study, O_2 still cracks the Pb−Br bonds. At the end of the simulations, the integrity ratio of Pb−Br connections is 62.50% (20/32), which is slightly higher than that of 58.33% (28/48) in the $CH_3NH_3PbI_3-O_2$ system and 43.75% (14/32) in the $(CH_3NH_3)_2Pb(SCN)_2I_2-O_2$ system. This indicates that the Pb−Br bonds are still not

https://doi.org/10.1021/acsomega.1c03952
ACS Omega 2021, 6, 24244−24255

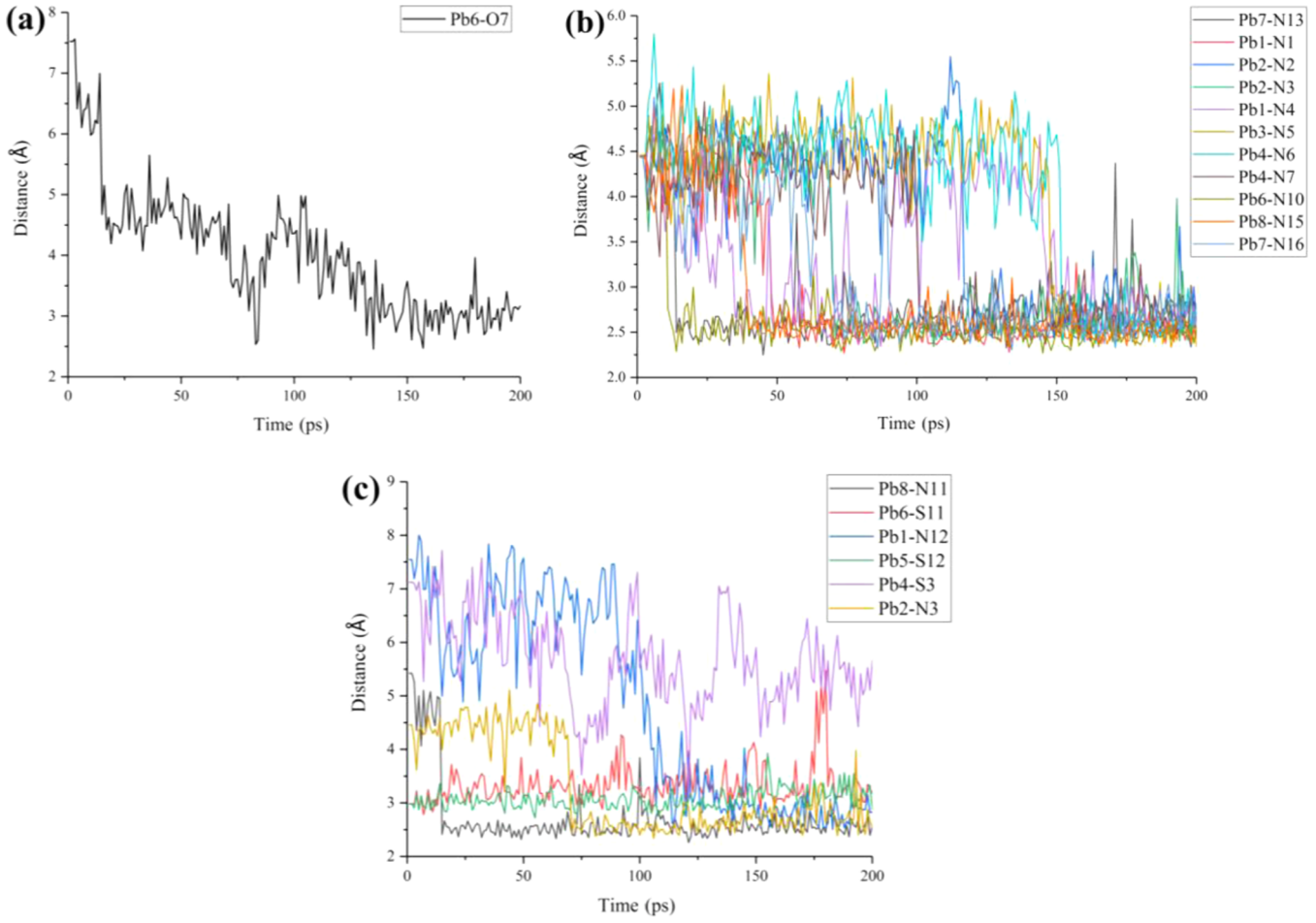

Figure 11. Evolution of the newly formed connections in the $Cs_2Pb(SCN)_2Br_2{-}O_2$ complex: (a) interaction of Pb−O, (b) connection of Pb−NCS, and (c) formation of Pb−SCN−Pb networks.

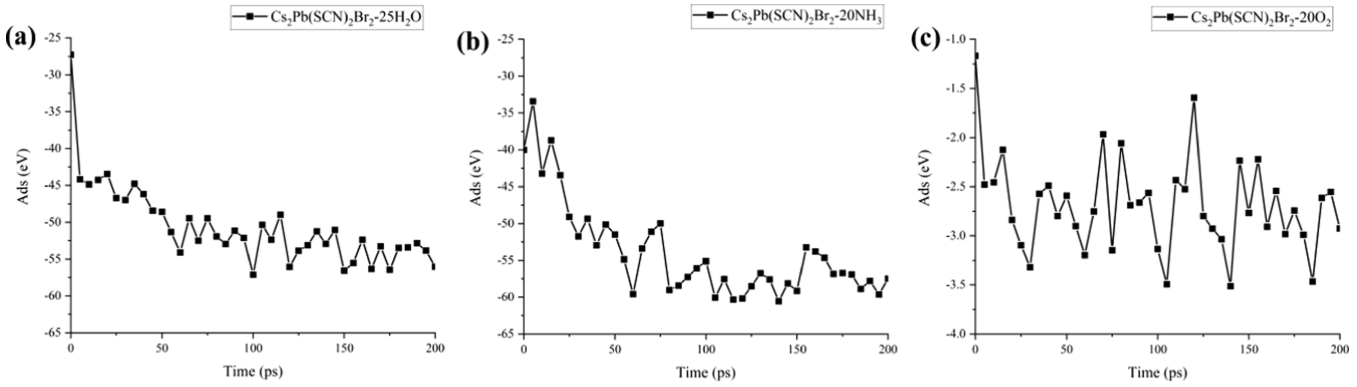

Figure 12. Adsorption energies of (a) $Cs_2Pb(SCN)_2Br_2{-}H_2O$, (b) $Cs_2Pb(SCN)_2Br_2{-}NH_3$, and (c) $Cs_2Pb(SCN)_2Br_2{-}O_2$ complex.

strong enough under strong oxidizing gas attacks. Despite this, in the $Cs_2Pb(SCN)_2Br_2{-}O_2$ system, the O_2 molecules are blocked and reside on the surface of perovskite materials and cannot enter the internal of the lattice throughout the simulations (Figure 9c), which is attributed to the contribution of the Pb−SCN (Figure 10b).

At the end of the dynamics process of the $Cs_2Pb(SCN)_2Br_2{-}O_2$ system, 11 out of 16 Pb−SCN transform to Pb−NCS connections, that is, Pb1−(NCS)1, Pb2−(NCS)2, Pb2−(NCS)3, Pb1−(NCS)4, Pb3−(NCS)5, Pb4−(NCS)6, Pb4−(NCS)7, Pb6−(NCS)10, Pb8−(NCS)15, Pb7−(NCS)-16, and Pb7−(NCS)13 (Figure 11b). In the $Cs_2Pb(SCN)_2Br_2{-}H_2O$ and $Cs_2Pb(SCN)_2Br_2{-}NH_3$ complexes, the number of Pb−NCS is 1 and 8, respectively. The reason of which is further analyzed in the following charge transfer section. In addition, the Pb6−(SCN)11−Pb8, Pb5−(SCN)-12−Pb1, and Pb4−(SCN)3−Pb2 networks are observed (Figure 11c, the normal bond length of Pb−S is 3.70 Å[43]). It is these special forms that are deemed to prevent O_2 molecules from entering the perovskite lattice, thus ensuring the structural integrity of the semiconductor materials.

https://doi.org/10.1021/acsomega.1c03952
ACS Omega 2021, 6, 24244−24255

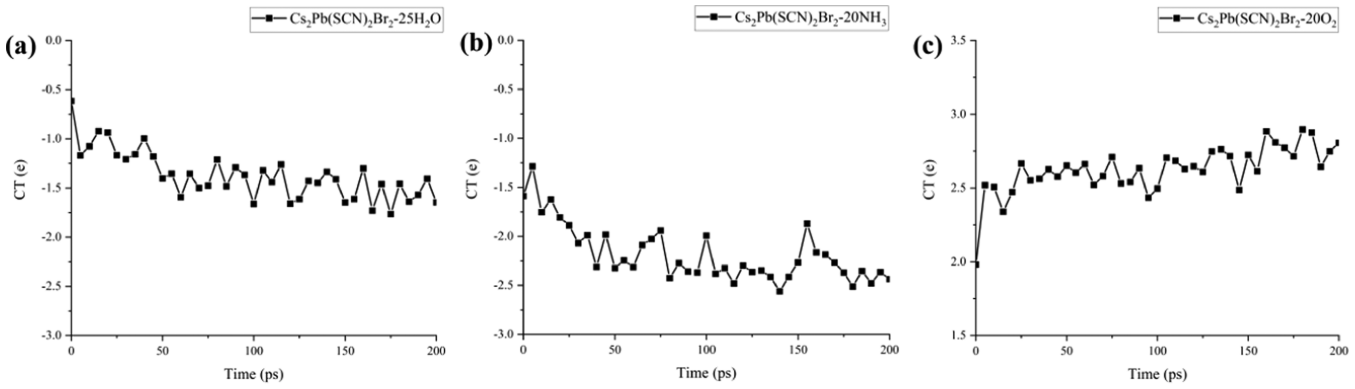

Figure 13. Charge transfer of (a) $Cs_2Pb(SCN)_2Br_2$−H_2O, (b) $Cs_2Pb(SCN)_2Br_2$−NH_3, and (c) $Cs_2Pb(SCN)_2Br_2$−O_2 complex.

From the above analyses, it can be seen that, during the adsorption processes, the −SCN groups on the $Cs_2Pb(SCN)_2Br_2$ surface are first affected by the gas molecules and different connections are detected, which is consistent with the RMSD curve fluctuations of the surface S, C, and N atoms.

The following quantitative data of the adsorption energy and charge transfer are used to depict the adsorption properties of the three systems.

2.4. Adsorption Ability of H_2O, NH_3, and O_2 on the $Cs_2Pb(SCN)_2Br_2$ Surface. Figure 12 and Table S1 demonstrate the data of the adsorption energies of the $Cs_2Pb(SCN)_2Br_2$−H_2O, $Cs_2Pb(SCN)_2Br_2$−NH_3, and $Cs_2Pb(SCN)_2Br_2$−O_2 complexes. The negative adsorption energy (E_{ad}) implies the reactions are exothermic and spontaneous. This indicates that the gas molecules are adsorbed on the $Cs_2Pb(SCN)_2Br_2$ surface; the larger adsorption energy suggests that more energy is released during the reaction and more stable connections are established. For the $Cs_2Pb(SCN)_2Br_2$−NH_3 system, in the initial phase of the dynamics process, the NH_3 molecules attack Pb atoms to form a stable Pb−N connection; however, the presence of Pb−SCN and Pb−NCS connections on the surface prevents more NH_3 molecules from attacking Pb atoms and the average adsorption energy of the system in the equilibrium stage is −57.611 eV. For the $Cs_2Pb(SCN)_2Br_2$−H_2O system, Pb atoms are still active sites that are first attacked by the H_2O molecules. Although the number of the newly formed Pb−OH_2 connections is larger than that of the Pb−N bonds mentioned above, the average adsorption energy of the system in the equilibrium stage is slightly lower, −53.678 eV. This is mainly due to the relatively weak Pb−OH_2 connections as discussed in Section 2.1. Furthermore, considering that the total number of H_2O molecules is 25 and that of NH_3 is 20, the adsorption ability of a single NH_3 is stronger than that of a single H_2O molecule. In contrast, the $Cs_2Pb(SCN)_2Br_2$−O_2 system is more special. Due to the frequent adsorption−desorption behaviors of O_2 in the dynamic process, the adsorption energy of the system is relatively lower than the above discussed two complexes, which is −2.781 eV. This phenomenon seems to fulfill the requirements of an ideal gas-sensing system, where the gas molecule under detection is not only easily adsorbed but also easily released from the sensing material surface.

2.5. Charge Transfer between $Cs_2Pb(SCN)_2Br_2$ and H_2O, NH_3, and O_2. Charge transfer is one of the most crucial factors influencing the resistivity of sensing materials. The calculated Bader charges are shown in Figure 13 and Table S2. In the initial stage, the quantity of the charge transfers from H_2O to $Cs_2Pb(SCN)_2Br_2$ is 0.616 e. In this case, both Pb^{2+} (−4.869 e) and Cs^+ (−9.870 e) in the $Cs_2Pb(SCN)_2Br_2$−H_2O system lose charges. The charges gained by SCN^- and Br^- are 7.967 e and 7.352 e, respectively. At the end of the dynamics process, the charge transferred from H_2O to $Cs_2Pb(SCN)_2Br_2$ is 1.647 e, and those of Pb^{2+}, Cs^+, SCN^-, and Br^- are −4.954 e, −9.913 e, 9.253 e, and 7.261 e, respectively. Therefore, during the dynamics processes, the donors in the $Cs_2Pb(SCN)_2Br_2$−H_2O system are H_2O (−1.031 e), Pb^{2+}(−0.085 e), Cs^+(−0.043 e), and Br^-(−0.091 e), respectively, while the acceptor is SCN^-(1.286 e). Similarly, for the $Cs_2Pb(SCN)_2Br_2$−NH_3 system, the donors are NH_3, Pb^{2+}, and Cs^+, donating −0.848 e, −0.141 e, and −0.088 e, respectively. The acceptors are SCN^- and Br^-, respectively, accepting 0.370 e and 0.714 e. In the $Cs_2Pb(SCN)_2Br_2$−O_2 complex, the donors are Pb^{2+} and Br^-, which separately provide −0.209 e and −0.708 e, respectively. The acceptors are O_2, Cs^-, and SCN^-, accepting 0.824 e, −0.150 e, and 0.244 e, respectively.

Pb^{2+} has both oxidizing and reducing properties. In the current work, Pb^{2+} loses charge, showing different degrees of reducibility, which may be related to the strong electron-withdrawing halogen or the pseudo-halogen groups connected with Pb^{2+}. In view of the formation of the multiple Pb−NCS connections and the strong electron-withdrawing capacity of the −CN groups, the relationship between the charge loss of Pb atoms and the number of Pb−NCS connections is proved, as shown in Table 1 and Figure 14. The data show that there is an obvious linear correlation between them in all three systems. Based on the above analysis, Pb^{2+} is a crucial active site and the gas molecules−Pb^{2+}−SCN^- connections are the main charge-transfer channels. Combined with the above structural stability analysis, although the stability of Pb−SCN and Pb−NCS is similar, considering the stronger electron-withdrawing properties of the −CN groups, more Pb−NCS connections indicate stronger electron-accepting ability during

Table 1. Relationship between the Loss of Charges of Pb Atoms and the Number of Pb−NCS Connections

$Cs_2Pb(SCN)_2Br_2$−H_2O		$Cs_2Pb(SCN)_2Br_2$−NH_3		$Cs_2Pb(SCN)_2Br_2$−O_2	
number of Pb−NCS connections	charge donated by Pb^{2+} (e)	number of Pb−NCS connections	charge donated by Pb^{2+} (e)	number of Pb−NCS connections	charge donated by Pb^{2+} (e)
4	−0.111	4	−0.060	4	0.011
3	−0.091	6	−0.071	7	−0.035
1	−0.085	8	−0.140	11	−0.227

https://doi.org/10.1021/acsomega.1c03952
ACS Omega 2021, 6, 24244−24255

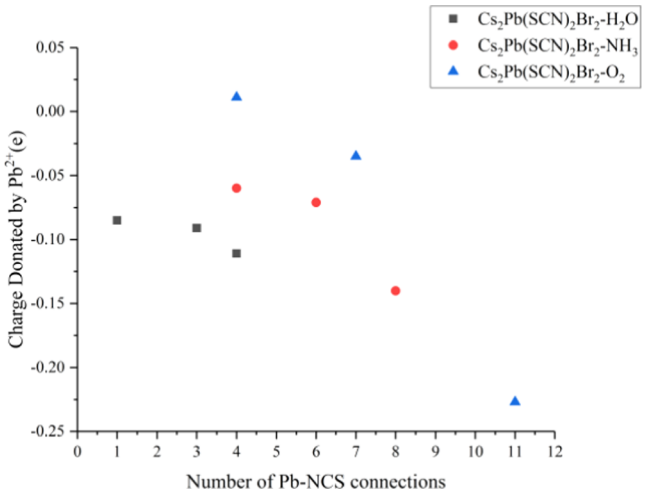

Figure 14. Relationship between the loss of charges of Pb atoms and the number of Pb−NCS connections.

the adsorption of various gas molecules. In the three systems, with the increase in the number of Pb−NCS bonds, Pb^{2+} loses more charge, showing stronger oxidizability. For the neutral H_2O and reductive NH_3, the systems receive charges. In terms of the strong oxidizing O_2, these systems still lose charges.

2.6. Influences on the Band Gap of $Cs_2Pb(SCN)_2Br_2$ from the Adsorption of H_2O, NH_3, and O_2. The band gap values of $Cs_2Pb(SCN)_2Br_2$ before and after the adsorption of the gas molecules were calculated and are listed in Table 2. To clearly show the band gap tuning of the semiconductor materials from gas sensing, the structures, in which the stable connections between the gas molecules and the surface of $Cs_2Pb(SCN)_2Br_2$ were formed (Figure S3), were selected and calculated. The band gap value of 0.794 eV refers to the pure perovskite material. After adsorption, as seen in Figure 13 and Table 2, when reductive NH_3 or neutral H_2O molecules were involved, $Cs_2Pb(SCN)_2Br_2$ receives charge from NH_3 or H_2O, the band gap increases; when oxidative O_2 molecules were absorbed, $Cs_2Pb(SCN)_2Br_2$ losses charge, the band gap decreases. It is well known that organometallic halide perovskites are ambipolar charge transporters due to the comparable effective masses of the electrons and holes.[44,45] The adsorption of both the electron-donating (NH_3 and H_2O) and the electron-withdrawing (O_2) molecules can increase the electron- and hole-doping level of $Cs_2Pb(SCN)_2Br_2$, causing the materials to behave as n- or p-type semiconductors.

Table 2. Band Gap Variations due to the Different Charge-Transfer Processes

$Cs_2Pb(SCN)_2Br_2-H_2O$		$Cs_2Pb(SCN)_2Br_2-NH_3$		$Cs_2Pb(SCN)_2Br_2-O_2$	
time (ps)	band gap (eV)	time (ps)	band gap (eV)	time (ps)	band gap (eV)
80	1.024	105	1.076	83	0.443
140	1.006	140	1.182	145	0.542
175	1.190	185	1.132	184	0.767

3. CONCLUSIONS

In the current work, the influences of the adsorption of typical neutral H_2O, reductive NH_3, and oxidative O_2 on the surface of $Cs_2Pb(SCN)_2Br_2$ on the perovskite geometric structures are investigated. The adsorption energy and charge-transfer processes between the gas molecules and semiconductor materials are calculated as well. The main conclusions are as follows:

(1) The Br^- doping, the Pb−NSC connection formation, and the replacement of the polar and stick-like $CH_3NH_3^+$ groups with the nonpolar and spherical CS^+ cations together can effectively improve the structural stability of the perovskite materials. The quick adsorption of the gas molecules on the $Cs_2Pb(SCN)_2Br_2$ surface and the fast charge transfer between them indicate ideal molecular recognition and, therefore, potentially high sensitivity to the three types of gas. When put in a humid or reductive gas environment, sensors based on $Cs_2Pb(SCN)_2Br_2$ are expected to present enhanced stability; however, under the attack of strong oxidizing gas molecules, the Pb−Br bonds are still not strong enough, which is a problem that warrants attention in the design of perovskite materials sensitive to strong oxidizing gases.

(2) Although the simulation time of 200 ps is still too short compared with the actual adsorption−desorption process, H_2O and NH_3 can be stably adsorbed on the surface of $Cs_2Pb(SCN)_2Br_2$ in the dynamics simulations, and no desorption is observed. The electrons flow from the gases to the semiconductor materials. O_2 is

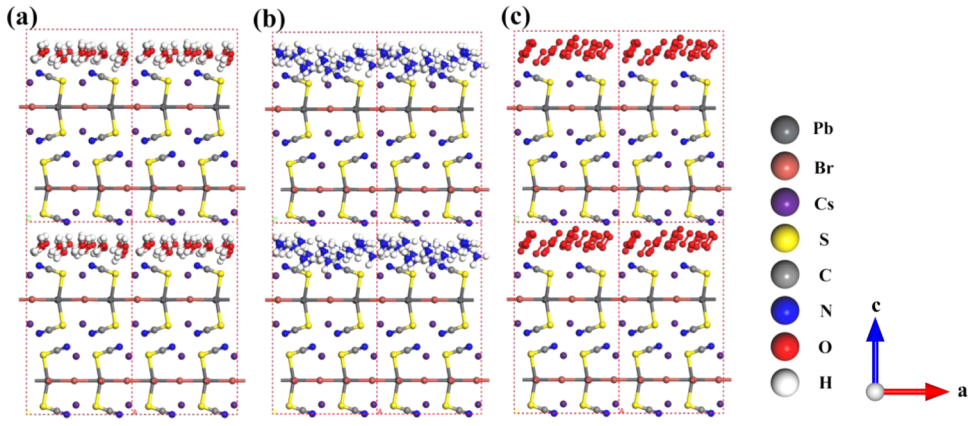

Figure 15. Initial structures of the three adsorption systems: (a) $Cs_2Pb(SCN)_2Br_2-H_2O$, (b) $Cs_2Pb(SCN)_2Br_2-NH_3$, and (c) $Cs_2Pb(SCN)_2Br_2-O_2$.

https://doi.org/10.1021/acsomega.1c03952
ACS Omega 2021, 6, 24244−24255

frequently adsorbed or desorbed, and the charge flows from the semiconductor materials to O_2. Based on these two different adsorption properties, the desorption properties of O_2 on the $Cs_2Pb(SCN)_2Br_2$ surface are more favorable to improving the recovery time of gas sensors.

(3) The simulations suggest when put in a humid or reductive gas environment, sensors based on $Cs_2Pb(SCN)_2Br_2$ are expected to present enhanced stability; however, under the attack of strong oxidizing gas molecules, the sensors can show high sensitivity but less stability than those in the neutral or reductive gases. This is because the Pb−Br bonds are still not strong enough, which is a problem that warrants attention in the future design of perovskite materials sensitive to strong oxidizing gases.

4. THEORETICAL METHODS

The modeling structure of $Cs_2Pb(SCN)_2Br_2$ was first optimized by Vienna ab initio simulation package (VASP),[46] which is built on the parent perovskite material $(MA)_2Pb(SCN)_2I_2$[47] crystal structure. Slabs of 2*2 from the bulk structure of $Cs_2Pb(SCN)_2Br_2$ were cut for $Cs_2Pb(SCN)_2Br_2-H_2O$, $Cs_2Pb(SCN)_2Br_2-NH_3$, and $Cs_2Pb(SCN)_2Br_2-O_2$ systems. The Cs^+-terminated (001)[48] perovskite surface was employed as the gas-exposed surface and a 5 Å vacuum space was set along the c-direction, which was filled with 25 H_2O, 20 NH_3, and 20 O_2 molecules, respectively (Figure 15). The cell lattice parameters a = 12.05, b = 12.55, and c = 21.98 Å for the complexes were used. In total, 163, 168, and 128 atoms are included in the $Cs_2Pb(SCN)_2Br_2-H_2O$, $Cs_2Pb(SCN)_2Br_2-NH_3$, and $Cs_2Pb(SCN)_2Br_2-O_2$ systems, respectively.

All of the ab initio dynamics simulations were carried out using the Car−Parrinello molecular dynamics (CPMD)[49] module in the Quantum-Espresso package.[50] Ultrasoft scalar relativistic pseudopotentials[51] and the generalized gradient approximation with the Perdew−Burke−Ezernhof (PBE) function[52] were applied describing the exchange interaction between atoms. Plane-wave basis set cutoffs for the augmented density and the smooth part of the wave functions are 200 RY and 25 RY, respectively. A fictitious electronic mass corresponds to 400 au. All of the dynamics calculations were conducted at a Nose−Hoover[53] constant temperature of 300 K. An integration time of 5 au was employed and the total simulation time was 200 ps for each system.

To describe quantitatively the influences of gas on the perovskite skeletons, the adsorption energy and charge transfer of the semiconductor−gas systems were computed every 5 ps. The structure optimization and comparisons of the stability of the Pb−SCN and Pb−NCS bonding were performed by the projected augmented wave (PAW)[54] plane-wave basis in VASP. The PBE calculations including the spin−orbit coupling (SOC)[55,56] were employed for all of the periodic complexes. The cutoff of the kinetic energy was set as 500 eV, and the electronic minimization was carried out with a tolerance of 10^{-4} eV. A Monkhorst−Pack k-point grid of 3 × 3 × 1 was applied for the convergence of the energies and forces of the three adsorption systems. To reflect accurately the geometry variations and the electronic states of the adsorbed gas molecules on the perovskite materials, all of the coordinates of the atoms in the snapshots were left unoptimized. The adsorption energy was computed via equation

$$E_{ad} = E_{(perovskite+gas)} - E_{perovskite} - E_{gas}$$

where E_{ad}, $E_{(perovskite+gas)}$, $E_{perovskite}$, and E_{gas} are the adsorption energy of the complex, the total structural energy of perovskite and gas, the total structural energy of perovskite, and the structural energy of gas, respectively. The nonlocal van der Waals (VDW) contributions were considered with Grimmer's DFT-D3 correction[57] to probe the interactions between $Cs_2Pb(SCN)_2Br_2$ and the gas molecules.

The Bader charge population analysis[58,59] was adopted to calculate the charge transfer between the gas molecules and the semiconductor material. The net charge transfer ΔQ is defined as follows

$$\Delta Q_X = Q_X^{t=200} - Q_X^{t=0}$$

where X represents Pb^{2+}, Br^-, SCN^-, Cs^+, or gas, respectively.

■ ASSOCIATED CONTENT

Supporting Information

The Supporting Information is available free of charge at https://pubs.acs.org/doi/10.1021/acsomega.1c03952.

The RMSD curves of $CH_3NH_3PbI_3-H_2O$ and $(CH_3NH_3)_2Pb(SCN)_2I_2-H_2O$; the final structure of $CH_3NH_3PbI_3-O_2$ and $(CH_3NH_3)_2Pb(SCN)_2I_2-O_2$ adsorption complexes; the snapshots with the stable connections between H_2O (a)−(c), NH_3 (d)−(f), and O_2 (g)−(i) and the surface of $Cs_2Pb(SCN)_2Br_2$, respectively; the adsorption energies of $Cs_2Pb(SCN)_2Br_2-H_2O$, $Cs_2Pb(SCN)_2Br_2-NH_3$, and $Cs_2Pb(SCN)_2Br_2-O_2$ adsorption complexes (PDF)

■ AUTHOR INFORMATION

Corresponding Author

Qiang Lu − *National Engineering Laboratory for Biomass Power Generation Equipment, North China Electric Power University, Beijing 102206, P. R. China; School of New Energy and State Key Laboratory of Alternate Electrical Power System with Renewable Energy Sources, North China Electric Power University, Beijing 102206, P. R. China;* orcid.org/0000-0002-4340-1803; Phone: +86 10 61772030; Email: qlu@ncepu.edu.cn, qianglu@mail.ustc.edu.cn; Fax: +86 10 61772032(801)

Authors

Bing Zhang − *National Engineering Laboratory for Biomass Power Generation Equipment, North China Electric Power University, Beijing 102206, P. R. China; School of New Energy and State Key Laboratory of Alternate Electrical Power System with Renewable Energy Sources, North China Electric Power University, Beijing 102206, P. R. China;* orcid.org/0000-0002-5758-0718

Xiaogang Wang − *School of New Energy, North China Electric Power University, Beijing 102206, P. R. China*

Yang Yang − *School of New Energy, North China Electric Power University, Beijing 102206, P. R. China*

Bin Hu − *National Engineering Laboratory for Biomass Power Generation Equipment, North China Electric Power University, Beijing 102206, P. R. China; School of New Energy and State Key Laboratory of Alternate Electrical Power System with Renewable Energy Sources, North China Electric Power University, Beijing 102206, P. R. China;* orcid.org/0000-0003-2801-9873

Lei Tong − *School of New Energy, North China Electric Power University, Beijing 102206, P. R. China*
Ying Liu − *School of New Energy, North China Electric Power University, Beijing 102206, P. R. China*
Li Zhao − *National Engineering Laboratory for Biomass Power Generation Equipment, North China Electric Power University, Beijing 102206, P. R. China; School of New Energy, North China Electric Power University, Beijing 102206, P. R. China*

Complete contact information is available at: https://pubs.acs.org/10.1021/acsomega.1c03952

Author Contributions

B.Z. contributed to the conception of the study, wrote the paper together with B.H., X.W., Y.Y., and L.T., and performed the simulations and data processing. Y.Y. and Y.L. performed the data analyses and figure preparation. L.Z. and Q.L. contributed to the constructive discussions and data analyses.

Notes

The authors declare no competing financial interest.

■ ACKNOWLEDGMENTS

The authors acknowledge support from the National Natural Science Foundation of China (51922040, 51821004, and 51876060), the Fundamental Research Funds for the Central Universities (2020DF01 and 2020MS161), and the China Postdoctoral Science Foundation (2020M680482).

■ REFERENCES

(1) Kojima, A.; Teshima, K.; Shirai, Y.; Miyasaka, T. Organometal halide perovskites as visible-light sensitizers for photovoltaic cells. *J. Am. Chem. Soc.* **2009**, *131*, 6050−6051.
(2) Wehrenfennig, C.; Eperon, G. E.; Johnston, M. B.; Snaith, H. J.; Herz, L. M. High charge carrier mobilities and lifetimes in organolead trihalide perovskites. *Adv. Mater.* **2014**, *26*, 1584−1589.
(3) Roldán-Carmona, C.; Malinkiewicz, O.; Soriano, A.; Espallargas, G. M.; Garcia, A.; Reinecke, P.; Kroyer, T.; Dar, M. I.; Nazeeruddin, M. K.; Bolink, H. J. Flexible high efficiency perovskite solar cells. *Energy Environ. Sci.* **2014**, *7*, 994−997.
(4) Zhou, H.; Chen, Q.; Li, G.; Luo, S.; Song, T. B.; Duan, H. S.; Hong, Z.; You, J.; Liu, Y.; Yang, Y. Interface engineering of highly efficient perovskite solar cells. *Science* **2014**, *345*, 542−546.
(5) Safdari, M.; Fischer, A.; Xu, B.; Kloo, L.; Gardner, J. M. Structure and function relationships in alkylammonium lead (ii) iodide solar cells. *J. Mater. Chem. A* **2015**, *3*, 9201−9207.
(6) National Renewable Energy Laboratory, Best Research-cell Efficiency Chart, 2021, https://www.nrel.gov/pv/cell-efficiency.html (accessed Seven 2021).
(7) Conings, B.; Drijkoningen, J.; Gauquelin, N.; Babayigit, A.; D'Haen, J.; D'Olieslaeger, L.; Ethirajan, A.; Verbeeck, J.; Manca, J.; Mosconi, E.; Angelis, F. D.; Boyen, H. G. Intrinsic thermal instability of methylammonium lead trihalide perovskite. *Adv. Energy Mater.* **2015**, *5*, No. 1500477.
(8) Xing, J.; Liu, X. F.; Zhang, Q.; Ha, S. T.; Yuan, Y. W.; Shen, C.; Sum, T. C.; Xiong, Q. Vapor phase synthesis of organometal halide perovskite nanowires for tunable room-temperature nanolasers. *Nano Lett.* **2015**, *15*, 4571−4577.
(9) Dai, J.; Zheng, H.; Zhu, C.; Lu, J.; Xu, C. Comparative investigation on temperature-dependent photoluminescence of $CH_3NH_3PbBr_3$ and $CH(NH_2)_2PbBr_3$ microstructures. *J. Mater. Chem. C* **2016**, *4*, 4408−4413.
(10) Park, B. W.; Seok, S. I. Intrinsic Instability of Inorganic−Organic Hybrid Halide Perovskite Materials. *Adv. Mater.* **2019**, *31*, No. 1805337.
(11) Zhao, Y.; Zhu, K. Optical bleaching of perovskite $(CH_3NH_3)PbI_3$ through room-temperature phase transformation induced by ammonia. *Chem. Commun.* **2014**, *50*, 1605−1607.
(12) Bao, C.; Yang, J.; Zhu, W.; Zhou, X.; Gao, H.; Li, F.; Fu, G.; Yu, T.; Zou, Z. A resistance change effect in perovskite $CH_3NH_3PbI_3$ films induced by ammonia. *Chem. Commun.* **2015**, *51*, 15426−15429.
(13) Stoeckel, M. A.; Gobbi, M.; Bonacchi, S.; Liscio, F.; Ferlauto, L.; Orgiu, E.; Samori, P. Reversible, fast, and wide-range oxygen sensor based on nanostructured organometal halide perovskite. *Adv. Mater.* **2017**, *29*, No. 1702469.
(14) Kakavelakis, G.; Gagaoudakis, E.; Petridis, K.; Petromichelaki, V.; Binas, V.; Kiriakidis, G.; Kymakis, E. Solution processed $CH_3NH_3PbI_{3-x}Cl_x$ perovskite based self-powered ozone sensing element operated at room temperature. *ACS Sens.* **2018**, *3*, 135−142.
(15) Gupta, N.; Nanda, O.; Grover, R.; Saxena, K. A new inorganic-organic hybrid halide perovskite thin film based ammonia sensor. *Org. Electron.* **2018**, *58*, 202−206.
(16) Jiao, W.; He, J.; Zhang, L. Synthesis and high ammonia gas sensitivity of (CH_3NH_3) $PbBr_{3-x}I_x$ perovskite thin film at room temperature. *Sens. Actuators, B* **2020**, *309*, No. 127786.
(17) Fu, X.; Jiao, S.; Dong, N.; Lian, G.; Zhao, T.; Lv, S.; Wang, Q.; Cui, D. A $CH_3NH_3PbI_3$ film for a room-temperature NO_2 gas sensor with quick response and high selectivity. *RSC Adv.* **2018**, *8*, 390−395.
(18) Ren, K.; Huang, L.; Yue, S.; Lu, S.; Liu, K.; Azam, M.; Wang, Z.; Wei, Z.; Qu, S.; Wang, Z. Turning a disadvantage into an advantage: synthesizing high-quality organometallic halide perovskite nanosheet arrays for humidity sensors. *J. Mater. Chem. C* **2017**, *5*, 2504−2508.
(19) Ganose, A. M.; Savory, C. N.; Scanlon, D. O. $(CH_3NH_3)_2Pb(SCN)_2I_2$: A more stable structural motif for hybrid halide photovoltaics? *J. Phys. Chem. Lett.* **2015**, *6*, 4594−4598.
(20) Zhang, B.; Zhou, S. J.; Tong, L.; Liao, Y. J.; Yi, J. X.; Qi, Y.; Yao, J. X. Large scale quantum dynamics investigations on the sensing mechanism of H_2O, acetone, NO_2 and O_3 adsorption on the $(MA)_2Pb(SCN)_2I_2$ surface. *Phys. Chem. Chem. Phys.* **2019**, *21*, 21223−21235.
(21) Tong, L.; Zhang, B.; Wang, X. G.; Liao, Y. J.; Yang, J. Q. Quantum dynamics simulations on the adsorption mechanism of reducing and oxidizing gases on the $CH_3NH_3PbI_3$ surface. *Adv. Theory Simul.* **2020**, *3*, No. 2000024.
(22) Li, C. H.; Tsai, C. C.; Liao, M. Y.; Su, Y. A.; Lin, S. T.; Chueh, C. C. Stable, color-tunable 2D SCN-based perovskites: revealing the critical influence of an asymmetric pseudo-halide on constituent ions. *Nanoscale* **2019**, *11*, 2608−2616.
(23) Chen, H.; Zhang, M.; Bo, R.; Barugkin, C.; Zheng, J.; Ma, Q.; Huang, S.; Ho-Baillie, A. W. Y.; Catchpole, K. R.; Tricoli, A. Superior self-powered room-temperature chemical sensing with light-activated inorganic halides perovskites. *Small* **2018**, *14*, No. 1702571.
(24) Wu, S.; Fan, Z.; Wang, W.; Fan, H.; Mei, Z.; Sun, D.; Cheng, X.; Zhao, X.; Tian, Y. Microfabricable ratiometric gaseous oxygen sensors based on inorganic perovskite nanocrystals and PtTFPP. *Sens. Actuators, B* **2018**, *271*, 104−109.
(25) Yamazoe, N.; Sakai, G.; Shimanoe, K. Oxide semiconductor gas sensors. *Catal. Surv. Asia* **2003**, *7*, 63−75.
(26) Kaewmaraya, T.; Ngamwongwan, L.; Moontragoon, P.; Jarernboon, W.; Singh, D.; Ahuja, R.; Karton, A.; Hussain, T. Novel green phosphorene as a superior chemical gas sensing material. *J. Hazard. Mater.* **2021**, *401*, No. 123340.
(27) Hussain, T.; Panigrahi, P.; Ahuja, R. Sensing propensity of a defected graphane sheet towards CO, H_2O and NO_2. *Nanotechnology* **2014**, *25*, No. 325501.
(28) Pannopard, P.; Khongpracha, P.; Probst, M.; Limtrakul, J. Gas sensing properties of platinum derivatives of single-walled carbon nanotubes: A DFT analysis. *J. Mol. Graphics Modell.* **2009**, *28*, 62.
(29) Lee, G. Y.; Yang, M. Y.; Kim, D. H.; Lim, J.; Byun, J.; Choi, D. S.; Lee, H. J.; Nam, Y. S.; Kim, I.; Kim, S. O. Nitrogen-Dopant-Induced Organic-Inorganic Hybrid Perovskite Crystal Growth on Carbon Nanotubes. *Adv. Funct. Mater.* **2019**, *29*, No. 1902489.

(30) Kim, S. J.; Park, Y. J.; Ra, E. J.; Kim, K. K.; An, K. H.; Lee, Y. H.; et al. Defect-induced loading of Pt nanoparticles on carbon nanotubes. *Appl. Phys. Lett.* **2007**, *90*, No. 023114.
(31) Goldoni, A.; Larciprete, R.; Petaccia, L.; Lizzit, S. Single-wall carbon nanotube interaction with gases: sample contaminants and environmental monitoring. *J. Am. Chem. Soc.* **2003**, *125*, 11329−11333.
(32) Collins, P. G.; Bradley, K.; Ishigami, M.; Zettl, A. Extreme oxygen sensitivity of electronic properties of carbon nanotubes. *Science* **2000**, *287*, 1801−1804.
(33) Peng, S.; Cho, K. Ab initio study of doped carbon nanotube sensors. *Nano Lett.* **2003**, *3*, 513−517.
(34) Kim, M. C.; Ahn, N.; Lim, E.; Jin, Y. U.; Pikhitsa, P. V.; Heo, J.; Kim, S. K.; Jung, H. S.; Choi, M. Degradation of $CH_3NH_3PbI_3$ perovskite materials by localized charges and its polarity dependency. *J. Mater. Chem. A* **2019**, *7*, 12075−12085.
(35) Mosconi, E.; Azpiroz, J. M.; Angelis, F. D. Ab Initio Molecular Dynamics Simulations of Methylammonium Lead Iodide Perovskite Degradation by Water. *Chem. Mater.* **2015**, *27*, 4885−4892.
(36) Zhang, L.; Yu, F.; Li, Q.; Su, J.; Li, J.; Li, M. Understanding interactions between halide perovskite surfaces and atmospheric/VOC gas molecules: an ab initio investigation. *J. Phys. D: Appl. Phys.* **2018**, *51*, No. 315302.
(37) Zhang, L.; Ju, M. G.; Liang, W. The effect of moisture on the structures and properties of lead halide perovskites: A first-principles theoretical investigation. *Phys. Chem. Chem. Phys.* **2016**, *18*, 23174−23183.
(38) Long, R.; Fang, W.; Prezhdo, O. V. Moderate humidity delays electron-hole recombination in hybrid organic-inorganic perovskites: Time-domain ab initio simulations rationalize experiments. *J. Phys. Chem. Lett.* **2016**, *7*, 3215−3222.
(39) Zhang, L.; Sit, P. H. L. Ab initio static and dynamic study of $CH_3NH_3PbI_3$ degradation in the presence of water, hydroxyl radicals, and hydroxide ions. *RSC Adv.* **2016**, *6*, 76938−76947.
(40) Zhang, B.; Liao, Y. J.; Tong, L.; Yang, Y. Q.; Wang, X. G. Ion migration in Br-doped $MAPbI_3$ and its inhibition mechanisms investigated via quantum dynamics simulations. *Phys. Chem. Chem. Phys.* **2020**, *22*, 7778−7786.
(41) Wells, A. F. *Structural Inorganic Chemistry*; Oxford University Press: Oxford, 2012.
(42) Geiger, D. K.; Parsons, D. E.; Zick, P. L. Crystal structures of three lead (II) acetate-bridged diaminobenzene coordination polymers. *Acta Crystallogr., Sect. E: Struct. Rep. Online* **2014**, *70*, 566−572.
(43) Pauling, L.; Kamb, B. *Linus Pauling: Selected Scientific Papers*; World Scientific: Singapore, 2001.
(44) Ball, J. M.; Lee, M. M.; Hey, A.; Snaith, H. J. Low-temperature processed meso-superstructured to thin-film perovskite solar cells. *Energy Environ. Sci.* **2013**, *6*, 1739−1743.
(45) Giorgi, G.; Fujisawa, J. I.; Segawa, H.; Yamashita, H. Cation role in structural and electronic properties of 3D organic-inorganic halide perovskites: A DFT analysis. *J. Phys. Chem. C* **2014**, *118*, 12176−12183.
(46) Kresse, G.; Furthmüller, J. Efficiency of ab-initio total energy calculations for metals and semiconductors using a plane-wave basis set. *Comput. Mater. Sci.* **1996**, *6*, 15−50.
(47) Daub, M.; Hillebrecht, H. Synthesis, Single-Crystal Structure and Characterization of $(CH_3NH_3)_2Pb(SCN)_2I_2$. *Angew. Chem., Int. Ed.* **2015**, *54*, 11016−11017.
(48) The original crystal structure of $(CH_3NH_3)_2Pb(SCN)_2I_2$ has been rotated 90 degrees counterclockwise around the B axis to keep exposed adsorption surface consistent with that of $MAPbI_3$ in one of our previous work. The built structure of $Cs_2Pb(SCN)_2Br_2$ in the current work is based on the rotated $(CH_3NH_3)_2Pb(SCN)_2I_2$ frame, the surface for adsorption is, therefore, (0 0 1).
(49) Car, R.; Parrinello, M. Unified approach for molecular dynamics and density-functional theory. *Phys. Rev. Lett.* **1985**, *55*, 2471−2474.
(50) Giannozzi, P.; Baroni, S.; Bonini, N.; Calandra, M.; Car, R.; Cavazzoni, C.; Ceresoli, D.; Chiarotti, G. L.; Cococcioni, M.; Dabo, I.; et al. QUANTUM ESPRESSO: a modular and open-source software project for quantum simulations of materials. *J. Phys.: Condens. Matter* **2009**, *21*, No. 395502.
(51) Laasonen, K.; Pasquarello, A.; Car, R.; Lee, C.; Vanderbilt, D. Car-Parrinello molecular dynamics with Vanderbilt ultrasoft pseudopotentials. *Phys. Rev. B* **1993**, *47*, 10142.
(52) Perdew, J. P.; Burke, K.; Ernzerhof, M. D. Generalized Gradient Approximation Made Simple. *Phys. Rev. Lett.* **1996**, *77*, 3865.
(53) Shuichi, N. Constant temperature molecular dynamics methods. *Prog. Theor. Phys. Suppl.* **1991**, *103*, 1−46.
(54) Blöchl, P. E. Projected augmented-wave method. *Phys. Rev. B* **1994**, *50*, 17953.
(55) Neese, F. Efficient and accurate approximations to the molecular spin-orbit coupling operator and their use in molecular g-tensor calculations. *J. Chem. Phys.* **2005**, *122*, No. 034107.
(56) Even, J.; Pedesseau, L.; Jancu, J. M.; Katan, C. Importance of Spin-Orbit Coupling in Hybrid Organic/Inorganic Perovskites for Photovoltaic Applications. *J. Phys. Chem. Lett.* **2013**, *4*, 2999−3005.
(57) Grimme, S.; Antony, J.; Ehrlich, S.; Krieg, H. A consistent and accurate ab initio parametrization of density functional dispersion correction (DFT-D) for the 94 elements H-Pu. *J. Chem. Phys.* **2010**, *132*, No. 154104.
(58) Sanville, E.; Kenny, S. D.; Smith, R.; Henkelman, G. Improved grid-based algorithm for Bader charge allocation. *J. Comput. Chem.* **2007**, *28*, 899−908.
(59) Tang, W.; Sanville, E.; Henkelman, G. A grid-based Bader analysis algorithm without lattice bias. *J. Phys.: Condens. Matter* **2009**, *21*, No. 084204.

https://doi.org/10.1021/acsomega.1c03952
ACS Omega 2021, 6, 24244−24255